Numerical analysis of the vacuum infusion process for sandwich composites with perforated core and different fiber orientations

Francisco J. Hurtado[1,*], Antonio S. Kaiser[1], Antonio Viedma[1] and Sebastián Díaz[2]

[1]Dpto. Ingeniería Térmica y de Fluidos, Universidad Politécnica de Cartagena, Doctor Fleming s/n, 30202 Cartagena, Spain

[2]MTorres Diseños Industriales S.A.U. Ctra. El Estrecho-Lobosillo, Km 2. 30320 - Fuente Álamo, Murcia, Spain

[*]Corresponding author. Tel. no.: +34 652 625 599. E-mail address: frnc.hurtado@gmail.com (F.J. Hurtado)

Abstract

The vacuum infusion is a process usually applied to manufacture large structures of composite materials**, such as wind turbine blades**. The specific stiffness and weight ratio required by these structures can be achieved by manufacturing sandwich composites. The forecast by numerical simulation of the resin infusion flow is an indispensable tool to design and optimize the manufacturing process of composite. Present work analyzes **by numerical simulation** the mold filling process of a sandwich composite, performed by fiberglass plies with different fiber orientations and a perforated core. The flow through a single perforation of the core is analyzed and the influence of the permeability values of fiberglass on the volume flow through core perforations is determined. In order to reduce the computing costs, a transfer function to simulate the flow through the perforations is developed and integrated in the numerical code by computational subroutines. **A 3D numerical modelling of a sandwich composite, in which the flow through the core perforations is simulated via computational subroutines, is carried out and experimentally validated.**

Keywords

Vacuum infusion, sandwich composites, perforated core, fiber orientation, computational modeling

Nomenclature

- C **Courant number**
- e wall distance (m)
- F surface tension volume force (kg m^{-2} s^{-2})
- g gravitational acceleration (m s^{-2})
- k permeability (m^2)
- $\bar{\bar{K}}$ permeability tensor (m^2)
- p pressure (N m^{-2})
- Q volume flow **(m^3 s^{-1})**
- r core perforation radius (m)
- S_D viscous loss term (kg m^{-2} s^{-2})

- S_χ volume source term of mass flow (kg s^{-1} m^{-3})
- t time (s)
- Δt **time step (s)**
- v_j average components of velocity (m s^{-1})
- V_C **mesh element volume (m^3)**

Greek symbols

- μ viscosity (kg m^{-1} s^{-1})
- ρ density (kg m^{-3})
- ϕ porosity, dimensionless
- χ **volume fraction, dimensionless**

Subscripts

- *11, 22* in-plane directions
- *33* through-thickness direction
- *a* air
- ***c*** **mesh element**
- ***in*** **inlet region**
- *r* resin
- ***out*** **outlet region**

Introduction

The fiber-reinforced plastics are composite materials which combine low weight, high mechanical strength and good corrosion resistance. Nowadays, the composite materials are widely used in the aerospace industry due to its characteristics and are **replacing** the traditional engineering materials. Vacuum infusion (VI), also called Liquid Resin Infusion (LRI), is a technology able to manufacture highly complex parts of composite materials with better control of properties, higher content of the reinforcing material, lower emissions of chemicals and lower cost than other processes. **Due to the advantages over the traditional resin transfer molding, VI is used in the manufacture of large components (Brouwer et al., 2003).** The manufacture of composite parts by VI is performed by the infusion of a thermoset resin in liquid state into a fiber material placed in a mold cavity sealed by a membrane or vacuum bag. The resin is forced into the mold since air is removed by a vacuum pump. The composite part is integrated by the fiber reinforcing material and the resin cured.

In composites for special applications, the fiber reinforcing material is set up by a laminate of multiple layers and the mechanical properties of the resulting composite depend on the stacking sequence of the laminate (order in which the plies with different orientations are stacked). Furthermore, for applications with specific requirements of stiffness and weight, as wind turbine blades, sandwich composites are manufactured **placing a core between two fiber reinforcing material layers**. **The resulting composite combines a high bending stiffness with a low weight**. The mechanical properties of several sandwich structure designs are studied in a large number of researches (Zhou and Stronge, 2005; Russo and Zuccarello, 2007).

The mold filling process must be designed in order to obtain a high quality product, decrease the mold filling time and achieve the successful and complete impregnation of the fiber material. Since the traditional trial-error methods are costly and time consuming, numerical simulation emerges as an effective alternative to design and to optimize the molding process. **To carry out an accurate numerical model, several experimental parameters, such as the resin properties and the porosity and permeability values of the fiber materials, must be determined. The permeability values of the reinforcing material is one of the most critical factors in setting the boundary conditions of the numerical model**, due to it determines the resin flow behavior during the mold filling stage. Since different experimental methods have been developed for the measurement of permeability values (Liu et al., 2007, or Endruweit and Ermanni, 2004, for instance), the standardization of procedure and deviation of measures are still under discussion (Vernet et al., 2014). The permeability is mainly dominated by the geometry of the porous media, which can vary considerably from point to point on a microscopic level. This variation can be a consequence of the manufacturing process, the handling of the material, the sample preparation or the compression rate **during the mold closing**. Hoes et al. (2002) show that the permeability is not a material property that can be characterized by one single value, but it exhibits a statistical distribution.

The macroscopic flow, the shape and location of gates and vents or the structural design of the mold can be analyzed through numerical models, which provide a prediction of the infiltration time, the resin flow front position, the pressure distribution and the velocity vectors inside the mold during the process. Several numerical models of the molding process to manufacture laminated composites **were carried out** (Grujicic et al., 2005; Dong, 2006; Montés and Sánchez, 2010). Nevertheless, a few studies about resin flow through sandwich composites can be found. Jun Ni et al. (1998) studied the resin flow in a sandwich composite with a grooved core designed to speed up the mold filling process. An analytic model for unidirectional flow advancement in a sandwich composite with fibrous core was presented by Song and Youn (2007). In relation to sandwich composites with perforated core, the influence of several holes patterns of the core on the mold filling time, weight increase, bending critical load and yield absorbed energy is studied experimentally by Halimi et al. (2003). A 2.5D numerical model for sandwich composites with perforated core and fibrous reinforcing material with isotropic permeability was carried out by Poodts et al. (2013).

Present work studies the flow of resin through a sandwich composite set up by multiple layers of anisotropic fibrous material, with different fiber orientations in the stacking sequence and a perforated core. **A 3D numerical simulation of the mold filling stage of a VI process for the manufacture of a sandwich composite is carried out**. The numerical results of flow front position on the distribution media and on the bottom ply of the composite are compared with the data obtained by an experimental test. The velocity and the pressure flow fields inside the mold are studied. The influence of permeability values on the volume flow through core perforations is determined. The numerical modelling of flow through the perforations of the core demands an excessive computing power, due to each independent resin flow front

inside each perforation must be calculated during the **transient computation**. To reduce the computational cost of the numerical model, a transfer function to simulate the flow through the core perforations **is** presented and introduced in the numerical code by computational subroutines. The aim of the numerical modelling is to provide a robust method for the optimization and analysis of resin infusion processes in the manufacture of complex or large three-dimensional sandwich composites, taking into account the perforated core and the different orientations of the plies.

2. Experimental research

To validate the numerical modelling proposed, experimental resin infusion during manufacture of a sandwich composite is performed. The vacuum infusion experimental system is shown in Figure 1. The reinforcing material preform is composed by a symmetric laminate of ten fiberglass layers and a perforated core of PET. **The resulting sandwich structure is** shown in Figures 1(b) and 1(c). Each fiberglass ply has a certain fiber orientation**, according to the stacking sequence:** [45º/-45º/0º/45º/-45º/PET core/-45º/45º/0º/-45º/45º]. **The core is a solid piece of PET material (15 mm thick) perforated with a square hole pattern. The transversal holes (3 mm diameter) are distanced 25 mm from each other. The PET core presents a total of 660 perforations**. A distribution media with high in-plane permeability is installed on the top of the preform to speed up the superficial resin flow. The runner is set to load the resin flow on the distribution media. The resin flow is driven from a storage tank to the runner through the inlet gate. The set is covered by a vacuum bag. The vent is installed in the contour of the lowest ply of the laminate. The resin infusion is leaded by removing the air inside the mold through a vacuum pump. The preform of reinforcing material is placed on a transparent rigid surface, in order to observe the infusion of resin through the bottom layer. The positions of the flow fronts in the top layer (on the distribution media) and in the bottom fiberglass ply are measured during the experimental molding process.

The experimental permeability values of the fiberglass plies and of the distribution media was obtained following the method proposed by Ferland et al. (1996). In order to avoid the inaccuracies in the permeability measure produces by the race tracking (Berg et al., 2014), **the edge of the fabrics was carefully sealed**. One of the most critical factors in the simulation of resin infusion processes is the setting of the permeability value of the reinforcing material in the through thickness direction. Although different methods (Scholz et al., 2007, for instance) are presented to determine it, there is a high difficulty to **obtain** the actual value of the permeability in the through thickness direction in infusion processes with flexible cover, due to its value is influenced by the fiber volume fraction, which is determined by the preform compaction. The computation of the permeability value as a function of the pressure field and of the preform compaction leads to calculate nonlinear equations in a non-steady domain and increases significantly the computation time. **In this work the perform compaction is not considered in order to reduce the computational cost of the model. The equivalent permeability of the fiberglass laminate in the through thickness direction was fitted numerically for the studied stacking sequence.**

Although the through-thickness permeability may be influenced by the stacking sequence in laminates of unidirectional fabrics (Sas et al., 2014), no significant differences were detected on the value of the permeability in the through thickness direction of the stacking **sequence** studied. The permeability values relative to the through thickness permeability ($3.5 \cdot 10^{-13}$ m^2) of the fiberglass fabric are shown in Table 1.

Experimental **test has** been developed under isothermal conditions. The epoxy resin, which made up the matrix of **the composite material**, has a density of 1,100 kg/m^3 and a viscosity of 0.25 Pa·s. A slow hardener curing agent is used, and the total curing time of the epoxy resin is six hours. A maximal variation of 5 % on the resin properties was detected during the first hour of reaction, so that the resin curing process becomes apparent after the mold filling stage.

Governing equations

Initial assumptions

As the experimental test was performed at constant temperature and the curing process of the resin starts in a significant way after the mold filling stage, the energy equation is not considered on the numerical model and the resin is assumed to be an incompressible non-reactive fluid, with constant properties during the infusion process. Assuming that the fabrics behind the resin flow front are saturated and due to the low Reynolds number of the flow during the infusion process, the resin flow can be modeled by the Darcy's law (Equation (1)) for porous media (Darcy, 1856).

$$\vec{v} = -\frac{k}{\phi \cdot \mu} \cdot \nabla p \qquad (1)$$

Where $\vec{v}$ is the resin velocity, k and ϕ are the permeability and porosity of the preform, μ is the dynamic viscosity of the resin and ∇p is the pressure gradient across the preform. Since the aim of the proposed model is to study the local effects in the resin flow front, the relaxation of the vacuum bag and the preform compaction are not taken into account, in order to reduce the computational cost of the model**. A** constant fiber volume fraction of 53 % for the fiberglass **and 20 %** for the distribution media is considered. Furthermore, no effect of draping in the permeability values has been considered, as the experimental tests were flat.

The governing equations of the flow within the fluid domain are the Navier-Stokes ones. To get an accurate simulation of the flow the governing equations are solved for the fluid velocity (not for the averaged or Darcy's velocity), and the porosity of the porous media is taken into account in the continuity and momentum equations. According to the exposed assumptions, the interface tracking between the air and the resin is governed by a continuity equation for the volume fraction of the resin (Equation (2)).

$$\frac{1}{\rho_r}\left[\frac{\partial}{\partial t}(\chi_r \phi \rho_r) + \nabla(\chi_r \phi \rho_r \overrightarrow{v_r}) = \overrightarrow{S_{\chi_r}}\right] \quad (2)$$

Where $\overrightarrow{S_{\chi_r}}$ is the volume source term of resin mass flow, whose purpose will be defined in section *Model of core perforation with transfer function (model B)*.

A single momentum equation is solved throughout the domain, and the resulting velocity field is shared among the phases. The momentum equation (Equation (3)) is dependent on the volume fraction of the resin by means of density and viscosity properties.

$$\frac{\partial}{\partial t}(\phi\ \rho\ \vec{v}) + \nabla(\phi\ \rho\ \vec{v}\ \vec{v}) = -\phi \nabla \mathrm{p} + \nabla[\phi\mu(\nabla\vec{v} + \nabla\vec{v}^T)] + \phi\ \rho\ \vec{g} + \phi\ \vec{F} + \overrightarrow{S_D} \quad (3)$$

where $\vec{F}$ is the surface tension force modeled by the method proposed by Brackbill et al. (1992), and $\overrightarrow{S_D}$ is the viscous loss term, corresponding to the Darcy's law and defined by Equation (4).

$$\overrightarrow{S_D} = -\frac{\phi^2 \mu}{k} \cdot \vec{v} \quad (4)$$

When the resin flow through the perforations of the PET core is reproduced in the numerical simulations, the source term $\overrightarrow{S_D}$ is considered equal to zero and the porosity ϕ equal to one in Equations (2) and (3), within the free fluid domain (not filled with porous media) at the core perforations.

Fiber orientation modeling

The resin flowing through the reinforcement material during the mold filling stage is mainly dominated by the pressure gradient inside the mold, which is determined by the geometry of the piece, the locations of the gates and vents and the permeability values of the different fabrics that make up the laminate. In order to model correctly the permeability of the laminate, some considerations must be made. Each of the fiberglass plies that form the stack (taken individually) is an anisotropic porous material with the permeability tensor given by a diagonal matrix if the principal axis (eigenvectors of the linear relation between pressure gradients and flow velocity) are taken as the reference system. This diagonal tensor $\overline{\overline{K}}$ is formed by the permeability (eigenvalues) of the layer in the three principal axis (*11, 22, 33*), according to Equation (5).

$$\overline{\overline{K}} = \begin{bmatrix} k_{11} & 0 & 0 \\ 0 & k_{22} & 0 \\ 0 & 0 & k_{33} \end{bmatrix} \quad (5)$$

When a stack set up by plies with different fiber orientations is studied globally, a common reference system (*x*, *y*, *z*) must be used. To solve the governing equations in

plies where the fiber orientations do not match with the common reference system, a permeability tensor in the directions of the common reference system must be calculated. This permeability tensor $\overline{\overline{K'}}$ is obtained by a change of basis matrix *Q*, as showed in Equation (6).

$$\vec{v}_{(11,22,33)} = -\frac{1}{\phi \cdot \mu} \cdot \overline{\overline{K}} \cdot \nabla p_{(11,22,33)} \rightarrow \vec{v}_{(x,y,z)} \cdot Q = -\frac{1}{\phi \cdot \mu} \cdot \overline{\overline{K}} \cdot Q \cdot \nabla p_{(x,y,z)} \quad (6)$$

For instance, a ply with the principal axis oriented 45º to the common reference system, as depicted in Figure 2, will have **a change of basis matrix *Q* given by Equation (7)** and a permeability tensor given by Equation (8).

$$\boldsymbol{Q} = \begin{bmatrix} \frac{\sqrt{2}}{2} & \frac{-\sqrt{2}}{2} & \mathbf{0} \\ \frac{\sqrt{2}}{2} & \frac{\sqrt{2}}{2} & \mathbf{0} \\ \mathbf{0} & \mathbf{0} & \mathbf{1} \end{bmatrix} \quad \textbf{(7)}$$

$$\overline{\overline{K'}} = Q^{-1} \cdot \overline{\overline{K}} \cdot Q = \begin{bmatrix} \frac{k_{11}+k_{22}}{2} & \frac{k_{11}-k_{22}}{2} & 0 \\ \frac{k_{11}-k_{22}}{2} & \frac{k_{11}+k_{22}}{2} & 0 \\ 0 & 0 & k_{33} \end{bmatrix} \quad (8)$$

For this layer, taken as an example, the flow velocity and the pressure gradient are no longer parallel vectors and the relationship between them is given by Equation (9).

$$\vec{v} \begin{cases} v_x = -\frac{1}{\phi \cdot \mu} \cdot \left(\frac{k_{11}+k_{22}}{2} \cdot \frac{\partial p}{\partial x} + \frac{k_{11}-k_{22}}{2} \cdot \frac{\partial p}{\partial y} \right) \\ v_y = -\frac{1}{\phi \cdot \mu} \cdot \left(\frac{k_{11}-k_{22}}{2} \cdot \frac{\partial p}{\partial x} + \frac{k_{11}+k_{22}}{2} \cdot \frac{\partial p}{\partial y} \right) \\ v_z = -\frac{k_{33}}{\phi \cdot \mu} \frac{\partial p}{\partial z} \end{cases} \quad (9)$$

To reproduce this effect in a laminate formed by plies of different orientations stacked together, the discretization used in the numerical modelling must conserve the same structure and the cells **(elements of the discretized domain)** must defined in layers matching the actual plies, with the aim to define different porous media for each ply of the laminate. In this way, the permeability tensor used in each porous media will be defined according to the process presented to plies with 45º orientation, and the actual effect of the pressure gradient on the flow velocity vector will be reproduced in each point.

Numerical modeling

The numerical modelling of the vacuum infusion process of sandwich composites with perforated cores usually demands a prohibitive computing power, due to the fact that

a high number of elements in the discretization of the computational domain **are** required to obtain an accurate numerical simulation of the flow through each perforation of the PET core. In addition, an individual resin flow front for each perforation at the plies below the core must be calculated, as a result of the infusion through the perforated core. **Therefore, in order to reduce the computational cost of the numerical model, the flow through a single perforation of the core during the mold filling stage is analyzed to develop a transfer function able to simulate the presence of the core perforations in the computational domain.** The transfer function carried out determines the flow through each perforation of the core as a function of the conditions at their inlet and outlet sections. The adequate integration of the transfer function in the numerical code avoids the modelling of the volume of the perforations in the computational domain. To carry out an appropriate description of the process, the computational domain and boundary conditions of the different numerical simulations developed are introduced in this section. On the other hand, the analysis of flow through a single perforation, the set up and **the** integration in the numerical code of the transfer function and the comparison of the results with experimental data will be exposed in the next section.

Computational domains

Firstly, a numerical model for a single perforation of the core (hereafter known as model of core perforation, or model *A*) is carried out to study the flow through the perforations during the mold filling process. The computational domain, shown in Figure 3, reproduces the core perforation and its inlet and outlet regions in the top and bottom sides of the fiberglass laminate. **According to the global VI process in the composite,** the entry section is considered on the top fiberglass ply and the exit section in the contour of the bottom ply.

Secondly, through the numerical results of the core perforation model, a transfer function able to calculate the flow through core perforations will be **determined**. Via the integration of the transfer function in the numerical code, through adequate computational subroutines, a numerical modelling for a single perforation of the core (hereafter known as model of core perforation with transfer function, or model *B*) is carried out. **In the model *B*** the presence of the core perforation is simulated by computational subroutines, so that the domain, shown in Figure 4, reproduces the top and bottom sides of the fiberglass laminate, but not the core perforation.

Finally, a numerical modelling of the experimental sandwich composite part (shown in Figure 1) is carried out (model *C*); the computational domain is shown in Figure 5. The domain reproduces the different components of the experimental setup: the inlet gate, the runner, the distribution media, the fiberglass preform ply by ply and the vacuum vent. The flow through each perforation of the PET core **(square hole pattern, hole diameter: 3mm and side dimension: 25 mm)** is simulated via computational subroutines, therefore the physical volume of each perforation is not considered in the domain.

Boundary conditions

The next boundary conditions are defined **in the domains** of the models for one single core perforation, model *A* and *B*, and **in the domain of the numerical modelling of the experimental system (model *C*).**

Entry/exit sections. The continuity condition is imposed in the entry section and outlet vent and the streamwise variations of velocity components are neglected. Experimental boundary conditions for relative pressure are used, corresponding to -10.971 Pa at the entry section (due to **height change** between the storage tank and the inlet section) and -101.325 Pa in the outlet vent.

Porous media. The distribution media and each ply of the laminate is modeled as an independent porous media according to the Darcy's law, defined by the porosity and permeability experimental values and the principal axes of permeability depending on the orientation of each ply. With the aim to reduce the computational time cost of the numerical model and to avoid the simulation of the free surface, the inlet gate and the runner are simplified by porous media. **Since the flow through these channels can be considered laminar during the infusion process, an equivalent permeability to reproduce the pressure drop calculated by the Poiseuille's law can be easily determined**. The results of modelling these channels as free fluid domains were compared with those obtained by its modelling as equivalent porous media; no significant influence on the infusion process was noted.

Core perforations. The physical volume of the core perforation is **discretized** in model *A*, therefore the resin flow through the free fluid domain of the core perforation is simulated numerically. On the other hand, in model *B* and in model *C*, the flow through the core perforations is **simulated** by source terms**, which are** calculated by the transfer function. The modelling of flow through core perforations by source terms is implemented in the numerical code through appropriate computational subroutines.

Walls. The no-slip boundary condition is imposed in the rigid mold, the vacuum bag and the perforated core. Due to the inlet gate and the runner are simplified as equivalent porous media, shear stress is considered equal to zero in the walls of these channels.

Initial conditions. To initialize the transient calculation, the channels and the porous media inside the mold cavity are considered under vacuum at the recorded conditions in the experimental test.

Numerical approach

The governing equations are discretized and solved numerically in the domains of the three numerical models presented by using the general-purpose code Fluent v.6.3.26 (FLUENT, 2006) **based on a finite volume procedure; several features have been**

changed by means of accessible subroutines. The equations are discretized using the PRESTO scheme, which is similar to the well-known staggered-grid scheme **(Patankar, 1980)**. To avoid the appearance of false diffusion, the results are achieved employing the linear third-order 'quick' scheme (Leonard, 1979). The SIMPLE algorithm **(Patankar and Spalding, 1972)** is used to solve the coupling between continuity and momentum equations through pressure.

Air and resin are considered as two immiscible fluids and the moving-boundary problem is solved under non steady conditions by a single set of momentum equations, tracking the volume fraction of each of the fluids throughout the domain by the volume of fluid model.

With regard to numerical convergence, for each time step, the criterion was $|(\xi^{i+1} - \xi^{i})/\xi^{i}| \leq 10^{-5}$, where ξ can stand for any of the dependent variables and i denotes the iteration number; besides the normalized residuals for mass and momentum variables for the full flow field had to be below 10^{-5}. **In order to limit the time step of the transient computation according to the characteristic time of the flow, the time step was calculated by Equation (10). The Courant number *C* was fitted to 0.25. The characteristic time Δt_c is calculated in each element of the discretized domain as the relation between the volume of the element and the volume flow rate across that element.**

$$\Delta t_{max} = C \cdot \Delta t_{c,min} \quad (10)$$

Structured, non-uniform meshes are employed to obtain the numerical results. A power-law distribution is applied to get fine meshing in the interface between the porous media and the free domain in order to avoid convergence problems and to simulate accurately the flow. The accuracy of the numerical results was tested by a grid dependence study. Several meshes were studied, up to 791.798 elements for the numerical modelling of the one single core perforation (model *A*). **Two parameters were considered to analyze the influence of the grid size: the volume flow and the pressure jump between inlet and outlet regions of the perforation. Table 3 shows that the volume flow is more sensitive to the grid size. Note that the Mesh 3 presents a deviation lower than 1 % regarding the absolute independence values.** The presented results are obtained by using a structured tetrahedral mesh integrated by 91.435 elements for the model *A*, 3.400 for the model *B* and by 464.663 for the numerical modelling of the VI process of the sandwich composite (model *C*).

Results and discussion

Model of core perforation (model A)

The pressure distribution and the velocity vectors on the **neighbouring regions** of the inlet and outlet sections of a **core perforation** are analyzed, through the numerical results of the **model *A***. The pressure contours when the domain is filled by resin are shown in Figure 6. The **regions** of the fiberglass laminate affected by the drain and

discharge effects, as a result of the presence of the core perforation, **comprise** three fiberglass plies adjacent to the inlet and outlet sections of the perforation.

Isosurfaces of velocity component v_z are show in Figure 7, it can be observed that the shape and size of drain and discharge regions are influenced by **the different fiber orientations of the stacking sequence**, thus the influence of permeability values over flow through core perforations must be studied. Furthermore, this influence can be observed in the evolution of resin flow front shape during the mold filling stage, as is shown in Figure 8. Resin flow front get an elliptical shape on the adjacent ply to the outlet section due to anisotropy of the fiberglass. Owing the stacking sequence of plies below the core (-45º, 45º, 0º), the elliptical shape is transformed into a circular one as the resin flow moves to the lower plies.

According to the nature of fluid at the inlet and outlet sections of the core perforation, the transient mold filling process can be divided in three stages. **The three stages can be observed analyzing the resin mass flow at inlet and outlet sections of the core perforation, show in Figure 9.**

Stage 1: The flow through the core perforation is air. **This stage starts** with the mold filling process and finishes when the resin flow arrives at the inlet of the perforation.

Stage 2: The resin flow front reaches the inlet section of the core perforation, but the flow at the outlet section is air. It lasts from the resin flow arrives at the inlet of the perforation until the resin comes out from the lower extreme of the perforation.

Stage 3: The flow through the core perforation is resin. The stage 3 extends from the resin flow starts to rise up in the outlet of the perforation until the end of the mold filling process.

The volume flow through the core perforation as a function of the pressure jump between the inlet and outlet **sections exhibits** different linear trends in each stage **(Figure 10)**, according to the properties of the different fluids at the inlet and outlet sections. The pressure jump keeps approximately constant during the stage 2, due to the low pressure loss along the perforation. However, the volume flow during stage 2 exhibits a linear trend in function of the pressure jump (Figure 10(b)), when the boundary condition of vacuum pressure at the outlet vent is changed.

Development of the transfer function

Via the study of the results of the model *A*, it is possible to develop a transfer function to determine the flow through the core perforation. **Due to the aim of the transfer function is to avoid the discretization of the volume of the core perforation, the actual inlet and outlet sections of the perforation will not be modeled in the discretized domain. In this way,** the transfer function must be able to calculate the volume flow as a function of the flow properties in the regions of the fiberglass plies adjacent to the inlet and outlet sections of the core perforation. In order to describe

the development of the transfer function, it is necessary to consider the next locations, depicted on Figure 11.

1. Inlet region: Section of the core perforation projected to the centroid of the neighbouring cells of the computational domain on the fiberglass ply adjacent to the inlet section.

2. Inlet section of the core perforation.

3. Resin flow front position inside the core perforation.

4. Outlet section of the core perforation.

5. Outlet region: Section of the core perforation projected to the centroid of the neighbouring cells on the fiberglass ply adjacent to the outlet section.

The pressure jump between inlet and outlet regions during the molding process can be modeled by the Darcy's law and by the Poiseuille's law. For instance, in the time of the molding process shown in Figure 11, the pressure jump can be calculated by adding the pressure loss in the inlet and outlet regions and the pressure loss inside the core perforation, according to Equations (**11**) to (**13**).

$$\Delta P_{15} = \Delta P_{12} + \Delta P_{23} + \Delta P_{34} + \Delta P_{45} \quad (11)$$

$$\Delta P_{15} = \frac{\mu_r \cdot L_{12}}{2 \cdot k} \cdot \frac{Q}{\pi \cdot r^2} + \frac{8 \cdot \mu_r \cdot L_{23}}{\pi \cdot r^4} \cdot Q + \frac{8 \cdot \mu_a \cdot L_{34}}{\pi \cdot r^4} \cdot Q + \frac{\mu_a \cdot L_{45}}{2 \cdot k} \cdot \frac{Q}{\pi \cdot r^2} \quad (12)$$

$$\Delta P_{15} = \left[(\mu_r \cdot L_{12} + \mu_a \cdot L_{45}) \frac{1}{2 \cdot k} + (\mu_r \cdot L_{23} + \mu_a \cdot L_{34}) \frac{8}{r^2} \right] \frac{Q}{\pi \cdot r^2} \quad (13)$$

Due to the pressure loss inside the core perforation is 10^{-4} times lower than the pressure loss in the inlet and outlet regions at any stage of behavior during the mold filling process (considering the experimental values of permeability), the terms associated to the tracking of resin flow front inside the core perforation (L_{23} and L_{34} in Equation (**13**)) can be considered negligible. Moreover, assuming that the air viscosity is negligible with respect to the resin viscosity, it is possible to obtain one equation valid for the three stages of behavior and the volume flow through the core perforations can be calculated by Equation (**14**).

$$Q = \frac{k \cdot \pi \cdot r^2}{\mu \cdot e} \cdot \Delta P_{15} \quad (14)$$

Where μ is the viscosity of the fluid in the inlet region and ***e*** takes different values in each stage. At stages 1 and 3, *e* is the sum of the thickness of the inlet and outlet regions (**$L_{12} + L_{45}$**), due to the same fluid is presented in both regions. On the other hand, at stage 2, *e* is the thickness of the inlet region (**L_{12}**), due to the pressure loss in the outlet region caused by the air flow can be considered negligible in front to that

caused in the inlet region by the resin flow. Considering the anisotropy of the fiberglass plies, Equation **(14)** may be expand to Equation (**15**) introducing the coefficients *a*, *b* and *c*.

$$Q = (a \cdot k_{11} + b \cdot k_{22} + c \cdot k_{33}) \cdot \frac{\pi \cdot r^2}{\mu \cdot e} \cdot \Delta \boldsymbol{P_{15}} \quad (\mathbf{15})$$

The numerical modelling of core perforation allows **studying** the influence of the permeability values on the volume flow through the core perforations. The correlation between volume flow rate through the core perforation and the permeability values of the fiberglass fabrics was studied by means of 120 cases resolved with the numerical modelling of core perforation (model *A*), in which the permeability values of fiberglass fabrics are changed within a range between 0.2 times and 10 times the actual experimental levels. The value of the coefficients *a*, *b* and *c* **can** be determined through a linear regression analysis of the results.

The standardized coefficients of the regression analysis, shown in Table 2, determines the relative weigh of each permeability over the ratio of the rest of the terms in Equation (**15**), the permeability of fiberglass in the through-thickness direction (k_{33}) presents the higher influence, with a weight of 80 %. The faster in-plane permeability k_{11} presents a weight of 12 %, and the slow in-plane permeability k_{22} presents a weight of 8 %. Figure 12 show the accuracy of the linear regression analysis in comparison with the numerical results.

The volume flow through the core perforation at each stage of behavior can be calculated as a function of fiber permeability values, the fluid viscosity and the pressure gap between its inlet and outlet regions by the presented transfer function. The coefficients obtained through the regression analysis remain constant during the infusion process for the studied configuration. Note that for different perforation dimensions, fiber plies thickness or stack sequences, new coefficients can be obtained by a similar procedure. The volume flow through core perforations can be calculated through Equation (**16**). The agreement between the transfer function (Equation (**16**)) and the numerical results of the model *A* at any stage was shown in Figure 10.

$$Q = (0.005 \cdot k_{11} + 0.0013 \cdot k_{22} + 1.83 \cdot k_{33}) \cdot \frac{\pi \cdot r^2}{\mu \cdot e} \cdot \Delta \boldsymbol{P_{15}} \quad (\mathbf{16})$$

Model of core perforation with transfer function (model B)

Since the volume flow through core perforations during the mold filling stage can be mathematically modeled, its numerical simulation can be simplified as long as the numerical code used allows introducing computational subroutines, which interact with the numerical resolution. The calculation of flow through core perforations are implemented in the numerical code through eight appropriate subroutines, written in the own programming language of the code (UDF, Fluent's User-Defined Function).

The integration of the subroutines in the numerical computation is shown in Figure 13. During the numerical computation, the subroutines execute the next processes.

1. *Data acquisition*: **The computational subroutines must define the different variables needed to implement the calculation of the volume flow through core perforations (i.e. pressure and volume fraction at inlet an outlet regions, fictitious volume of resin inside the perforation, time step and space coordinates). The subroutines identify the inlet and outlet regions of the core perforations by comparing the coordinates of the elements of the discretized domain with the coordinates of the core perforations according to the hole pattern dimensions.** The properties of flow in the regions of the fiberglass plies adjacent to the inlet and outlet sections of the core perforation are obtained. **The pressure in the inlet and outlet region is calculated as the volume average of the elements which compose these regions for each perforation. Thereby, the subroutines must compute and store the total volume for each inlet and outlet region, as the sum of the volumes of the elements of each region.**

2. ***Checking of the stage of behavior*** *and volume flow calculation*: The stage of behavior is determined according the fictitious volume of resin inside the perforation and the presence of resin in the inlet region. Depending on the stage of behavior, the volume flow of resin and air is calculated according to Equation (**16**). **Due to the fact that the presence of resin in the inlet region is not absolute, the volume fraction must be introduced in Equation (16), in order to ensure the numerical convergence when the resin flow is approaching to the inlet region. The volume fraction identifies the percentage of each phase in the elements of the numerical domain as a number between 0 and 1. In this way, the subroutines must to multiply the resulting volume flow in each element of the inlet region by the volume fraction in each element, according to Equation (17).**

$$Q_c = \chi_c \cdot \frac{V_c}{\sum_{in} V_c} \cdot (0.005 \cdot k_{11} + 0.0013 \cdot k_{22} + 1.83 \cdot k_{33}) \cdot \frac{\pi \cdot r^2}{\mu \cdot e} \cdot \Delta P_{15} \qquad (17)$$

3. *Source term*s setting: The volume flow through the core perforation is imposed **by the subroutines** in the mesh elements of the inlet and outlet regions by means of the **volume source term of mass flow**, S_χ, of resin and/or air in the continuity equation for the volume fraction (Equation (2)). **Accordingly, the volume source terms in the inlet region are calculated by Equation (18), taking into account the density of the phase and the volume of the element in which the term is imposed. The negative value of the source term at the inlet region indicates that it is a drain term of mass. In order to ensure the continuity through the perforation, the source terms in the outlet region is calculated as a function of the inlet source terms, according to Equation (19). The phase (air or resin) of the source term in the outlet regions is determined by the current stage of behavior.**

$$S_{\chi_{c,in}} = -\frac{1}{V_c} \cdot \rho \cdot Q_c \qquad (18)$$

$$S_{\chi_{c,out}} = (-1) \cdot \frac{1}{\sum_{out} V_c} \cdot \left(\frac{\sum_{in}(S_{\chi_r} \cdot V_c)}{\rho_r} + \frac{\sum_{in}(S_{\chi_a} \cdot V_c)}{\rho_a} \right) \cdot \rho \quad (19)$$

4. *Storage of variables*: Once the numerical computation of the current time step is converged, the fictitious volume of resin inside the perforation is calculated **according to** the volume flow through the perforation, the value of the current time step and the volume of resin accumulated inside the perforation in the previous time step. **This fictitious volume is storage for each perforation in order to identify the end of the stage 2, due to the filling of the perforation.**

The development of the computational subroutines allows **setting** up the numerical model *B*, in which the flow through the perforation is calculated **and imposed as source terms** by Equation (**18**). The results of the model *B* are compared with those obtained with the model *A* (**Figures 9 and** 14). The volume flow through the core perforation of the model *B* presents an average deviation lower than 1 % from the model with physical modelling of the perforation (model *A*). It can be observed the pressure and velocity component v_z in the fiberglass plies, above and below the perforated core, follow same trends in both models, with an average deviation of 1.5 % for the pressure and 8 % for the velocity component v_z.

Model of the experimental sandwich composite (model C)

A numerical modelling of the experimental sandwich composite is carried out via the computational code to simulate the perforations of the core. **The results of this transient model** provide the evolution of resin flow during the mold filling stage of the VI process. The numerical results are compared with those experimentally obtained. Experimental data and numerical result of resin flow front position depending on process time are shown in Figure **15 and Table 4**. It can be observed that the numerical results follow a same trend that the experimental results, with an average deviation of **3 %** for the flow front position on the distribution media and **6 %** for the flow front position on the bottom ply of the laminate.

The 3D multiphasic transient model reproduces with low deviation the resin flow front during the VI processes for sandwich composites, assuming that the curing process is negligible during the mold filling. The numerical modelling reproduces accurately the flow through core perforations. As shows Figure **16**, the influence of fiber orientations can be studied in the shape of resin flow front in the fiberglass plies below the perforated core. The numerical modelling allow the study of macro voids during the mold filling process, produced due to the design of the perforation pattern, which can derive in the discard of the composite part manufactured.

New numerical models to study the influence of the **pattern hole** design on the resin infusion process can easily performed by changing the coordinates of each core perforation in the computational subroutines. For instance, the resin flow in plies below the perforated core for a pattern hole of 75x75 mm is shown in Figure **16(b)**, at the same time of the mold filling process of the results showed in Figure **16(a) for a pattern hole of 25x25 mm**.

Conclusions

The flow through core perforations during the mold filling stage of the vacuum infusion process to manufacture a sandwich composite is studied. The influence of the anisotropy of the reinforcing material fibers and the orientation of each ply can be observed in the pressure contours, velocity vectors and shape of the resin flow front in the fiberglass layers above and below the perforated core. During the mold filling process, three stages can be observed according to the fluid nature presented in the inlet and outlet regions of each perforation. In each stage the volume flow through the core perforation present a linear tendency and can be calculated as a function of the pressure jump between inlet and outlet regions of the perforation, the properties of fluids and the properties of fiberglass plies. The influence of permeability values of fiberglass in the flow through core perforations is studied. The in-plane directions permeability (k_{11}, k_{22}) and the through-thickness permeability (k_{33}) of the fiberglass laminate present a relative weight over the ratio between the rest of terms of Equation (**16**) of 8 %, 12 % and 80 % respectively.

Several computational subroutines are carried out to simulate the presence of core perforations. The subroutines identify the nature and properties of flow in the inlet and outlet regions, which fit with the coordinates of each core perforation, calculate the volume flow as a function of pressure and flow characteristics and impose the inlet and outlet volume flow as source terms in these regions.

A 3D multiphasic transient numerical modelling for the mold filling stage of the VI process to manufacture sandwich composite materials with different fiber orientations is carried out. The numerical modelling is validated using data obtained through experimental tests. The numerical results provide the evolution of resin flow through the preform, the inlet mass flow, the pressure contours and the velocity vectors in each ply of the laminate during the mold filling process, and they predict the possible presence of macroscopic dry areas in the fiber reinforcement material. The three-dimensional modelling takes into account each fiberglass ply and the fiber orientations of the stacking sequence. The perforated core is simulated via a computational code, which calculates the flow through core perforations as a function of flow and fiberglass properties in the inlet and outlet regions of each perforation.

The simulation of core perforations through the computational code avoids the computation of the free surface of each independent resin flow front inside each perforation of the core and reduces the number of element of the computational domain by 90 %. **Furthermore, the dimensions of the mesh elements can be increased, due to the fact that the volume of core perforations is not discretized. In this way, the time step of the transient computation can be increased, according to the increment in the minimum characteristic time of the flow along the discretized domain.** The reduction of the computational cost enables the resin infusion analysis by numerical simulation of large parts of sandwich composites. Furthermore, the simulation of the perforated core via source terms allows performing different pattern

holes designs by the simple change of the coordinates of each core perforation in the computational subroutines.

Acknowledgements

The research work presented in this paper has been carried out under the project *"Automation of the global manufacturing process for wind turbine blades (AQ–BLADE)"* IDI-20110154, financially supported by Centro para el Desarrollo Tecnológico Industrial (CDTI) from the Spanish Government.

References

1. Brouwer WD, van Herpt ECFC and Labordus M. Vacuum injection moulding for large structural applications. Compos Part A: Appl Sci Manuf 2003; 34: 551-558.

2. Zhou D and Stronge WJ. Mechanical properties of fibrous core sandwich panels. Int J Mechanical Sciences 2005; 47: 775-798.

3. Russo A and Zuccarello A. Experimental and numerical evaluation of the mechanical behaviour of GFRP sandwich panels. Compos Structures 2007; 81: 575-586.

4. Liu Q, Parnas RS and Giffard HS. New set-up for in-plane permeability measurement. Compos Part A: Appl Sci Manuf 2007; 38(3): 954–62.

5. Endruweit A and Ermanni P. The in-plane permeability of sheared textiles. Experimental observations and a predictive conversion model. Compos Part A: Appl Sci Manuf 2004; 35(4): 439–51.

6. Vernet N et al. Experimental determination of the permeability of engineering textiles: Benchmark II. Compos Part A: Appl Sci Manuf 2014; 61: 172–184.

7. Hoes K, Dinescu D, Sol H, Vanheule M, Parnas RS, Luo Y and Verpoest I. New set-up for measurement of permeability properties of fibrous reinforcements for RTM. Compos Part A: Appl Sci Manuf 2002; 33: 959–969.

8. Grujicic M, Chittajallu KM and Walsh S. Non-isothermal preform infiltration during the vacuum-assisted resin transfer molding (VARTM) process. Appl Surf Sci 2005; 245: 51–64.

9. Dong CJ. Development of a process model for the vacuum assisted resin transfer molding simulation by the response surface method. Compos Part A: Appl Sci Manuf 2006; 37: 1316–1324.

10. Montés N and Sánchez F. A new computational tool for liquid composite moulding process design based on configuration spaces. Compos Part A: Appl Sci Manuf 2010; 41: 58–77.

11. Ni J, Li S, Sun X and Lee J. Mold filling analysis in vacuum-assisted resin transfer molding. Part II: SCRIMP based on grooves. Polym Compos 1998; 19(6): 818-829.

12. Song YS and Youn JR. Flow advancement through multi-layered preform with sandwich structure. Compos Part A: Appl Sci Manuf 2007; 38: 1082-1088.

13. Halimi F, Golzar M, Asadi P and Beheshty MH. Core modifications of sandwich panels fabricated by vacuum-assisted resin transfer molding. J Compos Mater 2003; 2013; 47 (15): 1853-1863.

14. Poodts E, Minak G, Dolcini E and Donati L. FE analysis and production experience of a sandwich structure component manufactured by means of vacuum assisted resin infusion process. Compos Part B: Eng 2013; 53: 179-186.

15. Ferland P, Guittard D and Trochu F. Concurrent methods for permeability measurement in resin transfer molding. Polymer composites 1996; 17: 149-158.

16. Berg DC, Dickert M, Meiners D and Ziegmann G. Influence of inaccuracies in permeability measurements. In: 16th European Conference on Composite Materials, Seville, Spain, 2014.

17. Scholz S, Gillespie JW and Heider D. Measurement of transverse permeability using gaseous and liquid flow. Compos Part A: Appl Sci Manuf 2007; 38: 2034–2040.

18. Sas HS, Wurtzel EB, Simacek P and Advani SG. Effect of relative ply orientation on the through-thickness permeability of unidirectional fabrics. Compos Sci Technol 2014; 96: 116–121.

19. Darcy H. Les Fontaines Publiques de la Ville de Dijon. Paris: Dalmont, 1856.

20. Brackbill JU, Kothe DB, Zemach C. A continuum method for modelling surface tension. J. Comput. Phys. 1992; 100: 335-354

21. FLUENT, 2006. FLUENT 6.3 User's Guide. FLUENT, Inc.

22. Patankar SV. Numerical Heat Transfer and Fluid Flow. Hemisphere, Washington, DC. 1980

23. Leonard BP. A stable and accurate convective modelling procedure based on quadratic upstream interpolation. Comp Meth Appl Mech Eng 1979; 19: 59-98.

24. Patankar S and Spalding D. A calculation procedure for heat, mass and momentum transfer in three-dimensional parabolic flows. Int. J. Heat Mass Transfer 1972; 15: 1787-1806.

Tables

Permeability	0º Orientation principal axes	Distribution media	Fiberglass fabric
k_{11}	*y*	7600	66
k_{22}	*x*	6570	46
k_{33}	*z*	5714	1

Table 1. Permeability tensor components. Relative values to the permeability in the through thickness direction of the fiberglass fabric.

Permeability	Coefficients	Coefficient of determination *R Square*	Durbin-Watson statistic
k_{11}	a = 0.005	0.998	1.7
k_{22}	b = 0.013		
k_{33}	c = 1.830		

Table 2. Correlation coefficients and accuracy of the regression linear analysis.

Magnitude	Mesh 1	Mesh 2	Mesh 3	Mesh 4	Mesh 5
Number of cells	57,615	77,907	91,435	228,088	791,718
Volume flow (m^3/s)	8.0e-9	8.9e-9	9.5e-9	9.6e-9	9.6e-9
Pressure jump ΔP_{15} (Pa)	6.7e+4	6.5e+4	6.3e+4	6.3e+4	6.3e+4

Table 3. Meshing influence study.

Distribution media			Bottom ply of the laminate		
Time (s)	Experimental (m)	Numerical (m)	Time (s)	Experimental (m)	Numerical (m)
30	0.175	0.156	60	0.025	0.020
90	0.260	0.253	120	0.125	0.100
180	0.333	0.339	210	0.205	0.190
270	0.387	0.402	300	0.265	0.255
330	0.420	0.437	390	0.324	0.307
450	0.478	0.500	420	0.367	0.321
540	0.520	0.539	570	0.408	0.388
630	0.557	0.577	660	0.440	0.426
690	0.580	0.593	750	0.468	0.458
720	0.593	0.603	870	0.508	0.508
840	0.608	0.620	990	0.555	0.574
960	0.623	0.640	1110	0.607	0.627
1080	0.640	0.658	1230	0.647	0.654
1200	0.660	0.669	1350	0.682	0.678
1320	0.675	0.678			

Table 4. Experimental data and numerical result of resin flow front position.

Captions for figures

Figure 1. Vacuum infusion process a) Experimental overview (Courtesy of MTorres). b) Assembly diagram, top view with fiber orientations c) Assembly diagram, central cross section.

Figure 2. Main directions of permeability versus space directions at plies with 45º orientation.

Figure 3. Computational domain of the model of core perforation, model A.

Figure 4. Computational domain of the model of core perforation with transfer function, model B.

Figure 5. Computational domain of the model of the experimental sandwich composite, model C.

Figure 6. Relative pressure when the domain is filled by resin. a) Isometric view of isosurfaces. b) Cross section at 0º orientation. c) Cross section at 45º orientation.

Figure 7. Velocity component v_z when the domain is filled by resin. a) Isometric view of isosurfaces. b) Cross section at 0º orientation. c) Cross section at 45º orientation.

Figure 8. Resin flow front shape in the outlet region of the core perforation at a certain time of the molding process.

Figure 9. Resin mass flow through the core perforation during the infusion process.

Figure 10. Volume flow through the core perforation as a function of the pressure jump. a) Stage 1 (Air at inlet and outlet). b) Stage 2 (resin at inlet and air at outlet) and stage 3 (resin at inlet and outlet).

Figure 11. Resin flow front at a certain time of the molding process.

Figure 12. Volume flow through the core perforation. Numerical results versus linear regression.

Figure 13. Flowchart of the numerical computation process.

Figure 14. Numerical results of model of core perforation vs. model of core perforation with transfer function. Results along the lengthwise axis of the perforation when the domain is filled by resin: b) Relative pressure c) Velocity component v_z.

Figure 15. Experimental data and numerical result of sandwich composite a) Flow front position on the distribution media. b) Flow front position on the bottom ply of the laminate.

Figure 16. Resin flow front positions in plies below perforated core, at 1 minute from the start of the mold filling process. a) Pattern hole of 25x25 mm. b) Pattern hole of 75x75 mm.

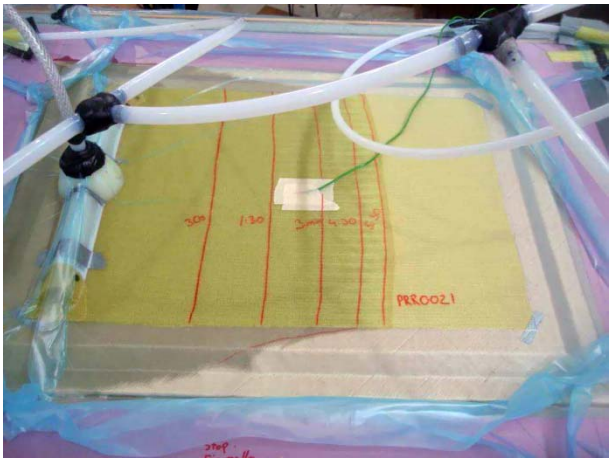

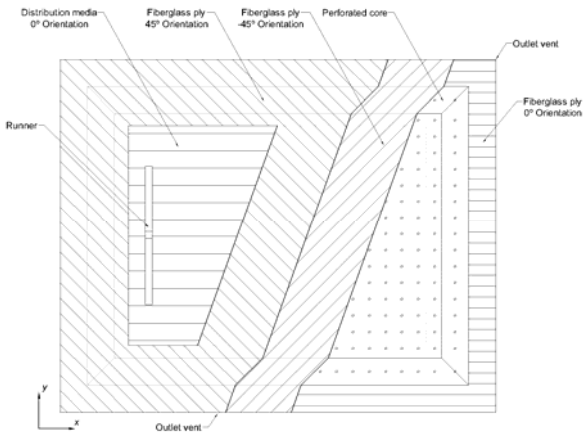

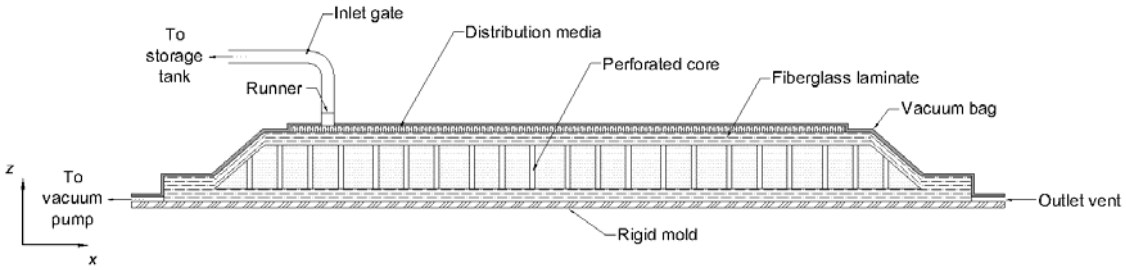

Figure 1. Vacuum infusion process a) Experimental overview (Courtesy of MTorres). b) Assembly diagram, top view with fiber orientations c) Assembly diagram, central cross section.

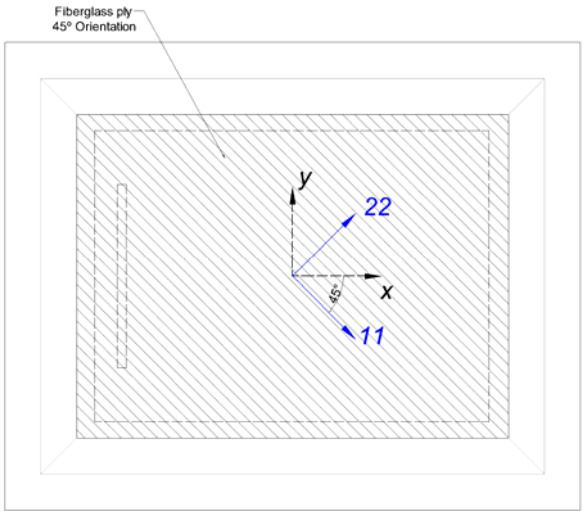

Figure 2. In-plane principal axis of permeability at plies with 45º orientation versus common reference system.

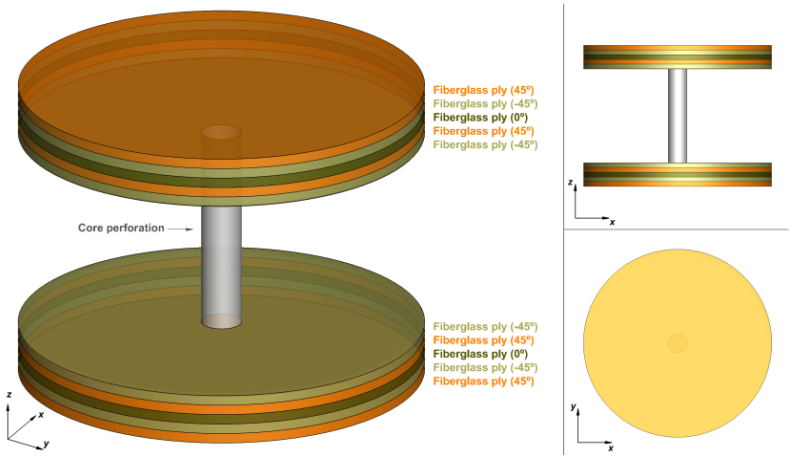

Figure 3. Computational domain of the model of core perforation, model A.

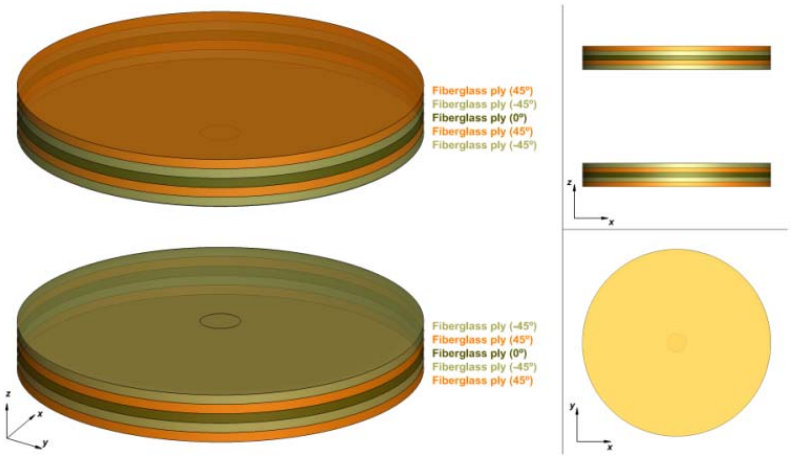

Figure 4. Computational domain of the model of core perforation with transfer function, model B.

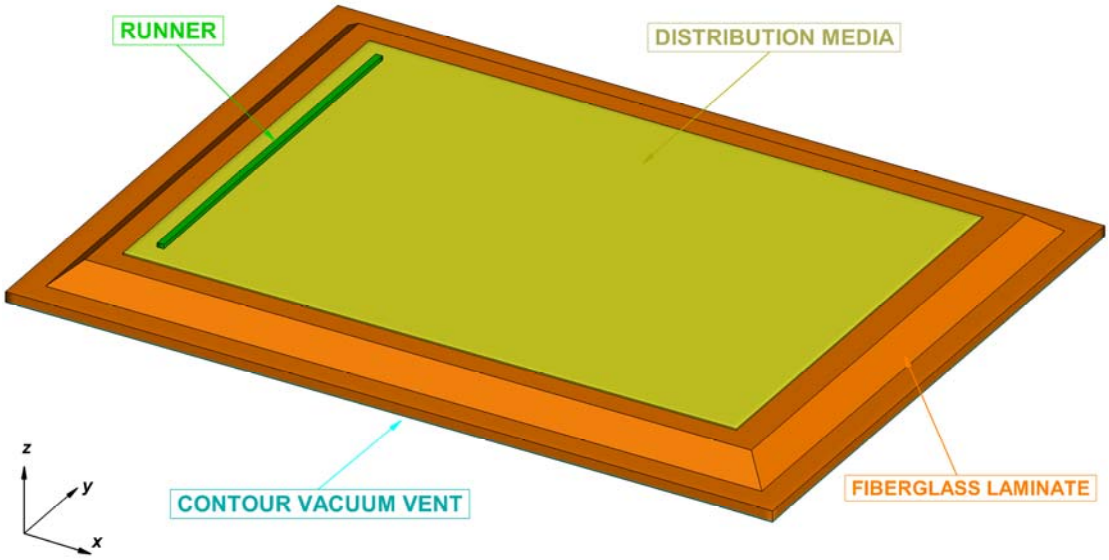

Figure 5. Computational domain of the model of the experimental sandwich composite, model C.

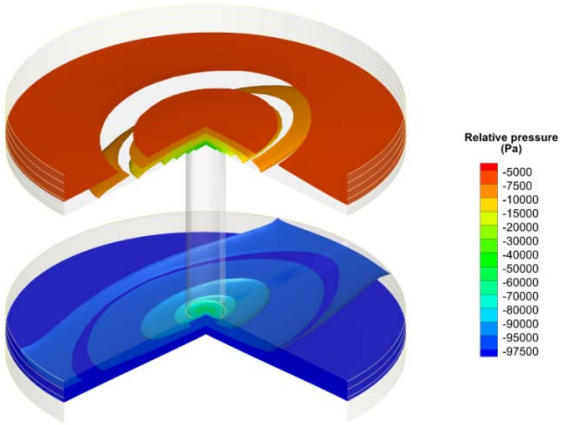

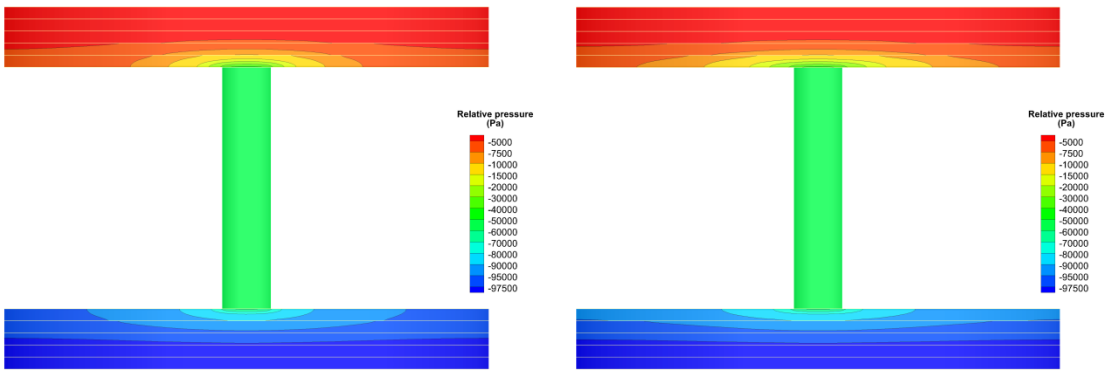

Figure 6. Relative pressure when the domain is filled by resin. a) Isometric view of isosurfaces. b) Cross section at 0º orientation. c) Cross section at 45º orientation.

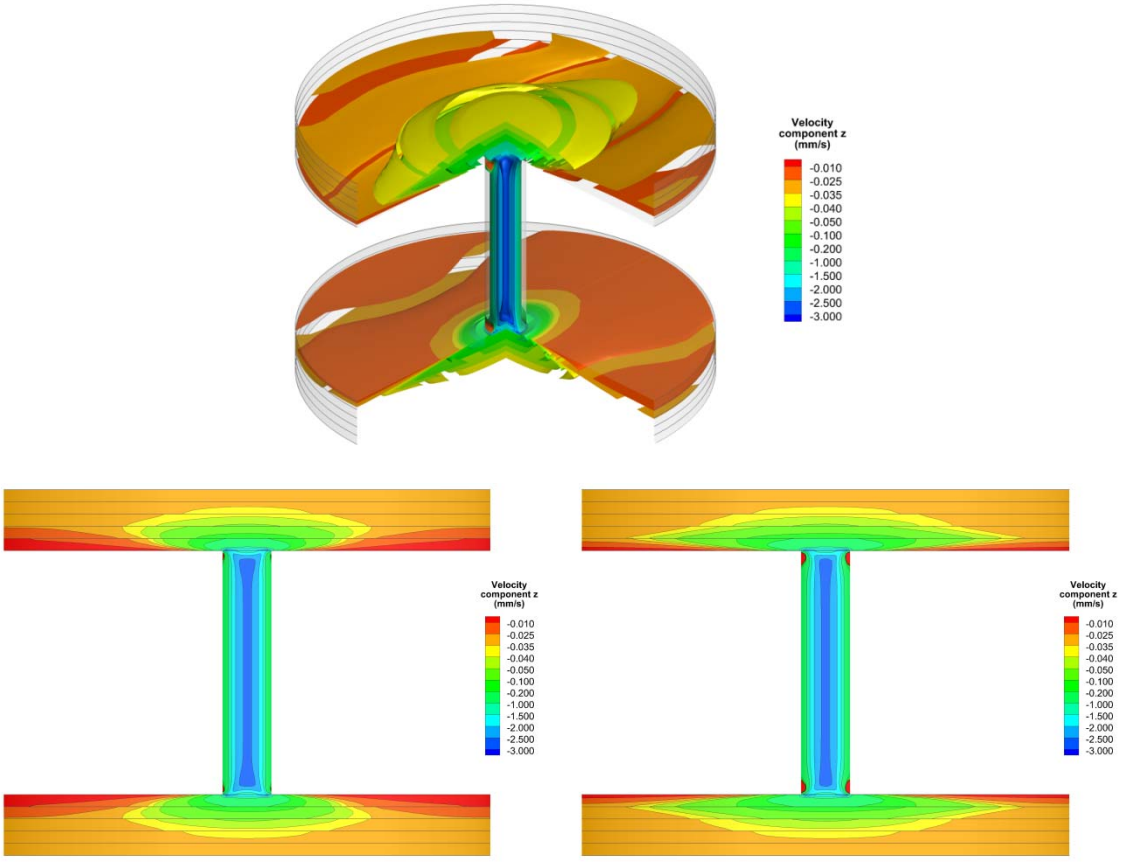

Figure 7. Velocity component v_z when the domain is filled by resin. a) Isometric view of isosurfaces. b) Cross section at 0º orientation. c) Cross section at 45º orientation.

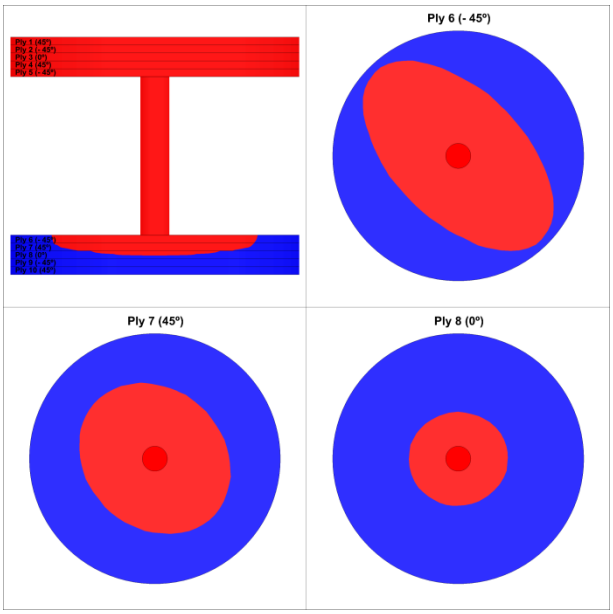

Figure 8. Resin flow front shape in outlet region of the core perforation at a certain time of the molding process.

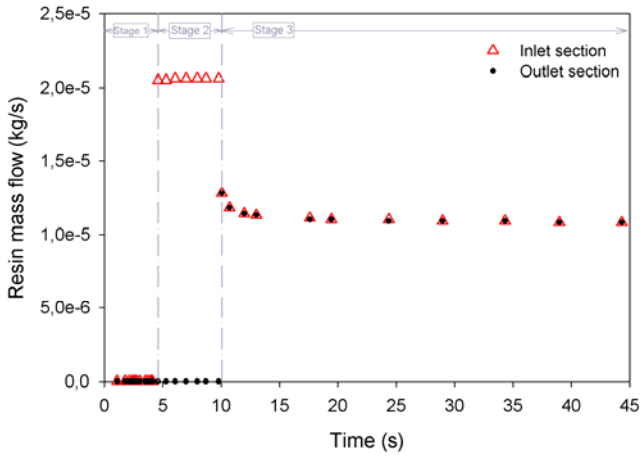

Figure 9. Resin mass flow at inlet and outlet sections of core perforation.

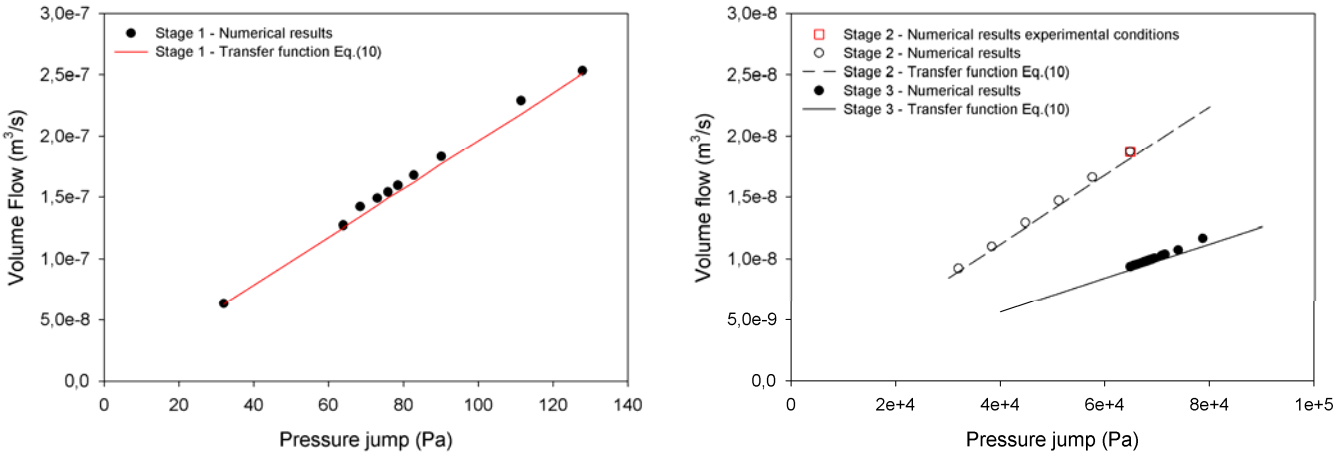

Figure10. Volume flow through the core perforation as a function of the pressure jump. a) Stage 1 (Air at inlet and outlet). b) Stages 2 (resin at inlet and air at outlet) and 3 (resin at inlet and outlet).

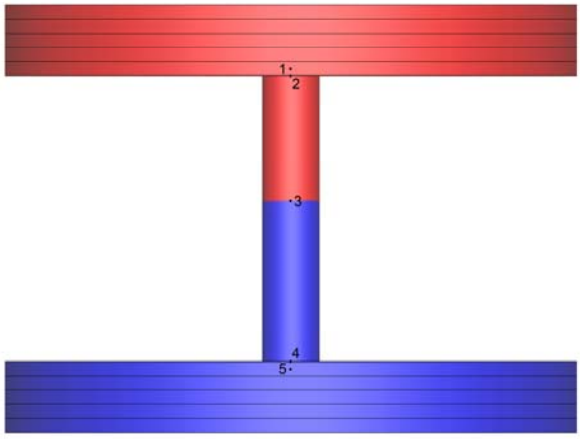

Figure 11. Resin flow front at a certain time of the molding process.

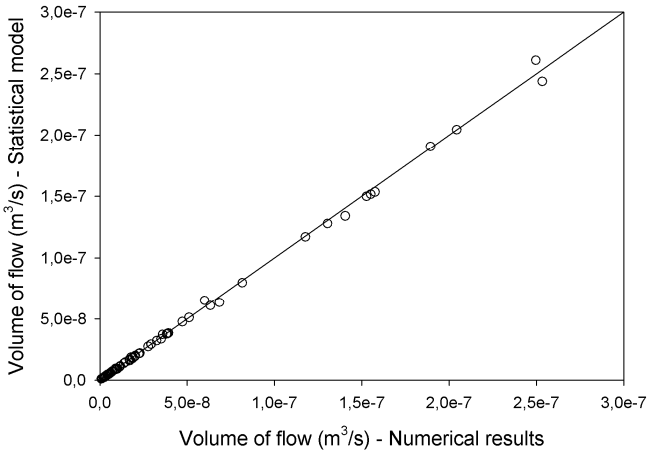

Figure 12. Volume flow through the core perforation. Numerical results versus linear regression.

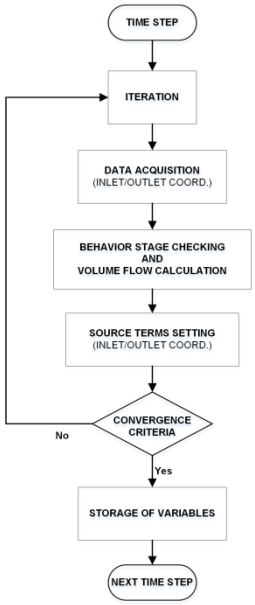

Figure13. Flowchart of the numerical computation process.

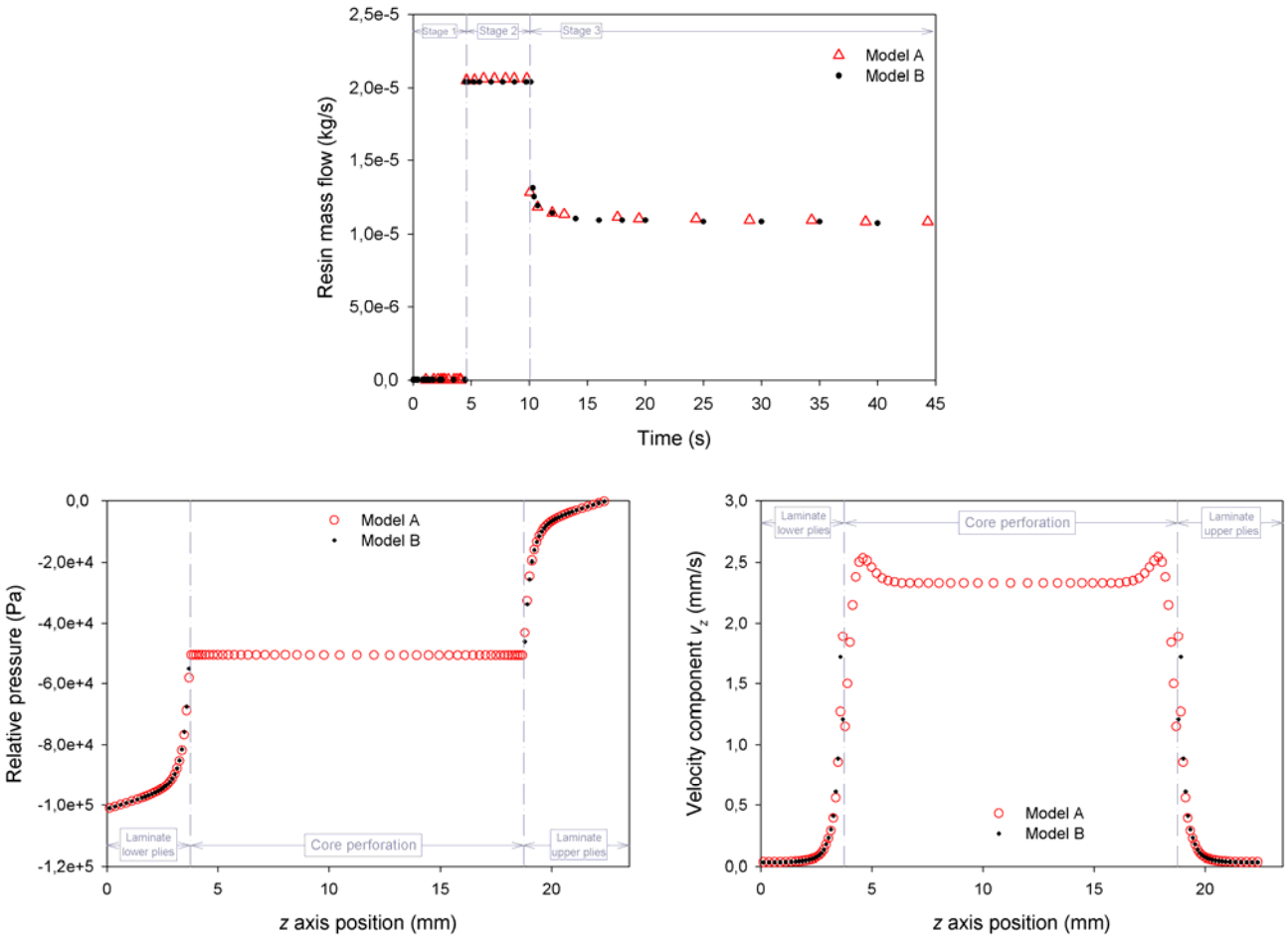

Figure 14. Numerical results of model of core perforation vs. model of core perforation with transfer function a) Resin mass flow at inlet section of core perforation during the mold filling process. Results along the lengthwise axis of the perforation when the domain is filled by resin: b) Relative pressure c) Velocity component v_z.

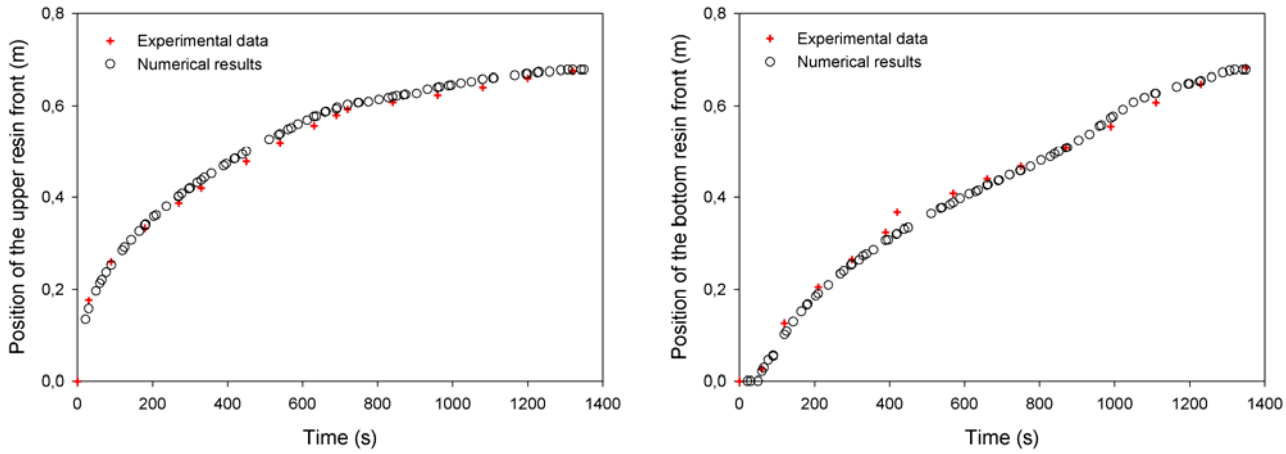

Figure 15. Experimental data and numerical result of sandwich composite a) Flow front position on the distribution media. b) Flow front position on the bottom ply of the laminate.

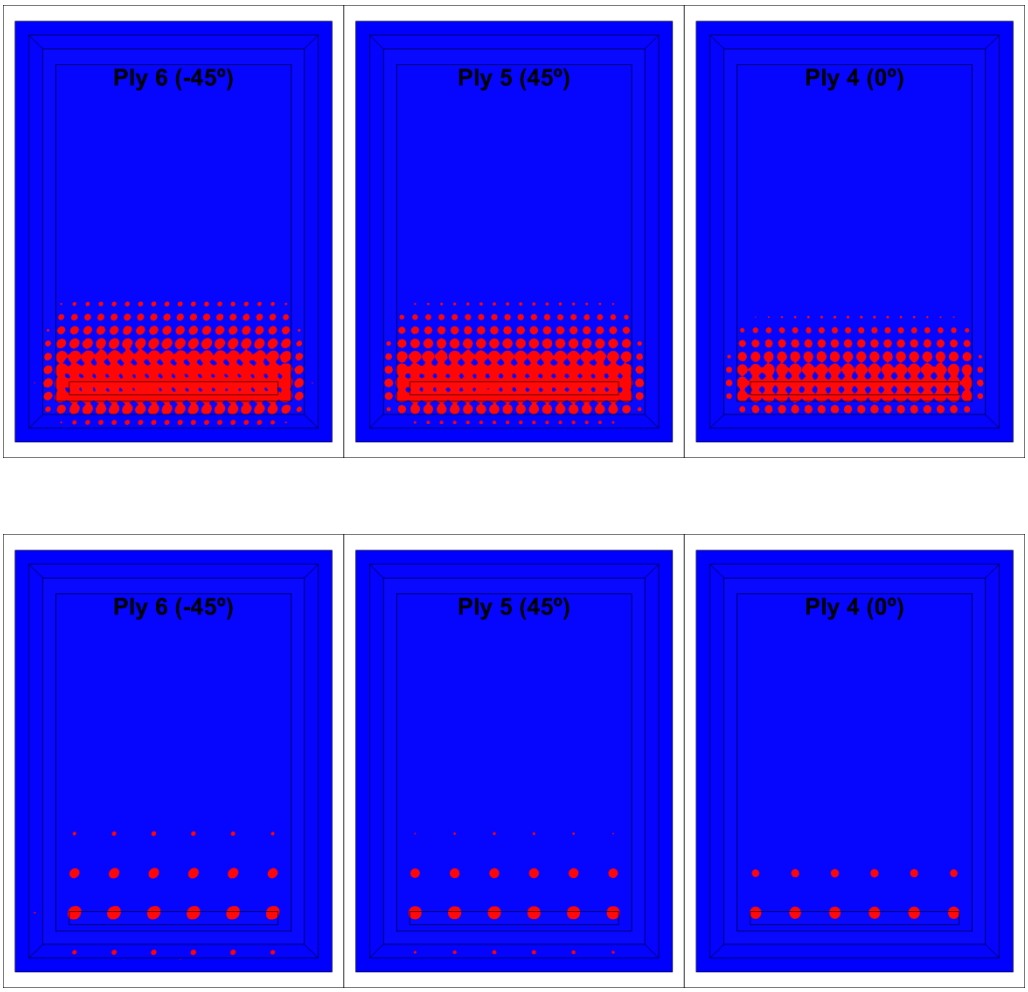

Figure 16. Resin flow front positions in plies below perforated core, at 1 minute from the start of the mold filling process. a) Pattern hole of 25x25 mm. b) Pattern hole of 75x75 mm.

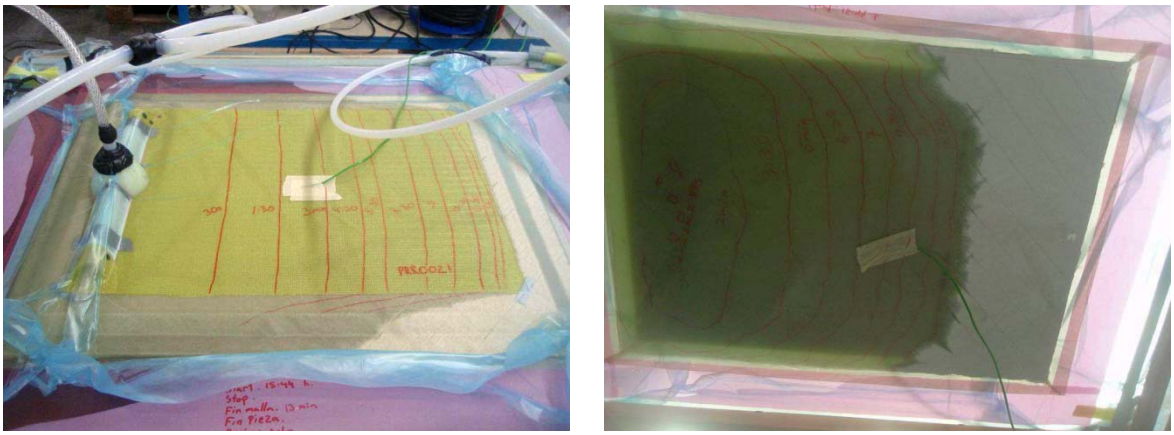

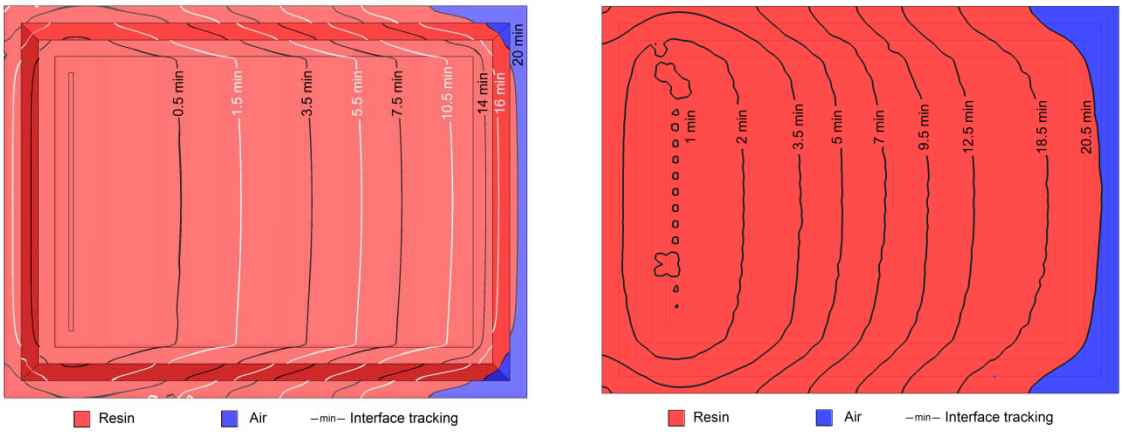

Missed Figure during revision: In-plane evolution of the resin flow front during the molding process. a) Experimental test on the distribution media (Courtesy of MTorres). b) Experimental test on the bottom ply (Courtesy of MTorres). c) Numerical results on the distribution media. a) Numerical results on the bottom ply.